Article

Electro-Oxidation of Humic Acids Using Platinum Electrodes: An Experimental Approach and Kinetic Modelling

Stefano Salvestrini [1,2], **Angelo Fenti** [3], **Simeone Chianese** [2,3,*], **Pasquale Iovino** [1,2] and **Dino Musmarra** [2,3]

[1] Department of Environmental, Biological and Pharmaceutical Sciences and Technologies, University of Campania "Luigi Vanvitelli", 81100 Caserta, Italy; stefano.salvestrini@unicampania.it (S.S.); pasquale.iovino@unicampania.it (P.I.)

[2] Environmental Technologies, University Spin off of University of Campania "Luigi Vanvitelli", 81100 Caserta, Italy; dino.musmarra@unicampania.it

[3] Department of Engineering, University of Campania "Luigi Vanvitelli", 81031 Aversa, Caserta, Italy; angelo.fenti@unicampania.it

* Correspondence: simeone.chianese@unicampania.it

Abstract: Humic acids (HA) are a potential hazard to aquatic ecosystems and human health. Because biological treatment of contaminated water does not satisfactorily remove these pollutants, novel approaches are under evaluation. This work explores electrochemical oxidation of HA in aqueous solution in a lab-scale apparatus using platinum-coated titanium electrodes. We evaluated the effects of HA concentration, current density, chloride concentration and ionic strength on the rate of HA oxidation. The initial reaction rate method was used for determining the rate law of HA degradation. The results showed that the reaction rate was first-order relative to HA concentration, chloride concentration and current density. An appreciable effect of ionic strength was also observed, most likely due to the polyanionic character of HA. We propose a kinetic model that satisfactorily fits the experimental data.

Keywords: humic acids; electro-oxidation; kinetic modelling; platinum electrodes; emerging and refractory pollutants; advanced oxidation processes (AOPs)

1. Introduction

The removal of emerging and refractory pollutants from wastewater is a priority research area worldwide [1,2]. Humic compounds are organic macromolecules deriving in nature from biological decomposition of organic matter [3]. They consist of aromatic and aliphatic blocks with carboxylic, phenolic and alkoxy functional groups [4,5]. Humic compounds are generally found in landfill leachate, as the organic fraction of mature leachate is mainly refractory humic substances [6–8], domestic sewage [9] and coking wastewater [10]. These are recalcitrant towards conventional biological treatment [11], thereby requiring additional treatment with other methods. Humic acids (HA) are the water-soluble fraction of humic compounds at neutral and basic pH [12]. HA impart undesirable color, taste, and odor to water [13] and are potentially harmful to aquatic ecosystems and human health [14–16].

Advanced procedures currently employed to remove recalcitrant compounds from wastewater include adsorption on conventional and innovative solid matrices [17–31], advanced oxidation processes (AOPs) [17,32–36], hydrodynamic cavitation [37,38], and ozone-based techniques [39–41]. In the last years, electrochemical oxidation (EO), a technique belonging to the class of AOPs, has proven to

be effective for removing bio-recalcitrant organic pollutants, due to the simplicity of operation, the stability, versatility, energy efficiency, easy handling, high removal efficiency and environmental compatibility [42–46].

Electrochemical oxidation consists in the application of an electrical potential difference at electrodes and involves two degradation mechanisms working either separately or simultaneously, depending on the nature of the electrodes [47–49]. These are (i) direct oxidation on the anodic surface via the generation of physically adsorbed hydroxyl radicals or chemisorbed reactive oxygen species and (ii) indirect oxidation by oxidants generated at the anode and freely diffusing in solution.

The performance of the EO technique strongly depends on operational conditions. The rate of degradation of organic compounds at low electrical potential increases using anodes with high electrocatalytic activity [48]. High electric current density [48,50] and electrolytes such as NaCl [48,51] enhance the oxidation rate, the former accelerating the generation of oxidants, the latter increasing the electrical conductivity of the solution. Moreover, chloride ions are known to produce reactive chlorine species that may take part in the oxidation process [52]. The pH also plays a relevant role because it affects the formation of oxidants such as OH radicals and reactive chlorine species [42].

Electrochemical oxidation has proven to be effective with several refractory pollutants such as phenol [42], organochlorine and organophosphorous pesticides [53], dyes [54] and cyanide [55]. Moreover, EO has been satisfactorily applied to the treatment of landfill leachate [6], coking wastewater [56], olive oil mill wastewater [57] and urine wastewater [58], as well as humics and humic-like substances [10,49,51,59–61].

Despite the strong interest in electro-oxidation applications, the current knowledge of chemical mechanisms underlying the process and of individual effects of a diversity of potential players remains incomplete. Here, we report an EO study on HA in a lab-scale experimental apparatus provided with platinum-coated titanium (Pt/Ti) electrodes. We worked on purified HA in artificial solutions and focused attention on the following variables: HA concentration, electric current density, inert and non-inert electrolytes, ionic strength and chloride ion concentration. The data were employed for the development and assessment of a kinetic model of the process.

2. Materials and Methods

2.1. Materials

HA were extracted from a compost sample using an acid/basic procedure [62,63]. The compost was purchased from Gesal S.r.l., Naples (Italy). According to the manufacturer's data, the sample contained 30% organic carbon and 1.7% organic nitrogen. All other chemicals employed in this study were from Sigma-Aldrich and were of analytical grade.

2.2. Humic Acids Extraction

One hundred grams of compost were treated with 1.0 L of distilled water and, under stirring, the pH was brought to 12.0 by dissolving solid NaOH. The mixture was stirred for two days and the pH periodically checked, adding a few drops of concentrated NaOH solution if necessary. The mixture was centrifuged at 10,000 rpm for 30 min, paper-filtered, and the filtrate recovered. After that, the pH was brought to 1.5 by adding concentrated HCl. After one night in the fridge, the precipitate was collected by centrifugation at 10,000 rpm, washed with distilled water and oven-dried at 45 °C. Eight grams of dry sample (henceforth denoted as HA) were obtained from 100 g compost, the yield of acid/basic extraction procedure thus being 8%.

For HA purification, a solution of raw HA at neutral pH was dialyzed against 0.1 M NaHCO$_3$ solution, using a molecular porous membrane tubing with a cut-off of 6–8 kDa (Spectra/Por), until UV–Vis absorbance of the external solution reached a stable value (approximately after one week).

2.3. Electro-Oxidation Experiments

Electro-oxidation experiments were carried out at lab scale at about 25 °C. A batch reactor of 0.5 L was fed with 250 mL of 70–150 mg L^{-1} HA solution (C_{HA}). The pH of the samples was recorded using a HI 9017 Hanna Instruments pH meter, calibrated in pH 1, 7 and 10 buffer solutions. The initial pH was brought to 10.0 by adding few drops of dilute NaOH solution. During the EO experiments, the pH was continuously monitored showing only a slight decrease, from 10.0 up to a minimum of about 9.0. These experimental conditions prevented the formation of HA aggregates [64,65].

The effect of reactive (Cl$^-$) and/or inert (ClO$_4^-$ or NO$_3^-$) anions was evaluated by adding 0.01–0.05 mol L^{-1} NaCl, NaClO$_4$ or NaNO$_3$ to the HA solution, which caused an increase of the ionic strength (*IS*) in the range 10–50 mM. The electrochemical reactor (Figure 1) consisted of two cylindrical electrodes of platinum-coated titanium 0.80 cm in diameter and 10 cm in length, placed at a distance of 3 cm. The electrodes were connected to a Direct Current (DC) power supply BPS-305 (Lavolta, London, UK). The EO tests were carried out under amperostatic conditions at values of current density (*I*) in the range 77–230 A m^{-2}.
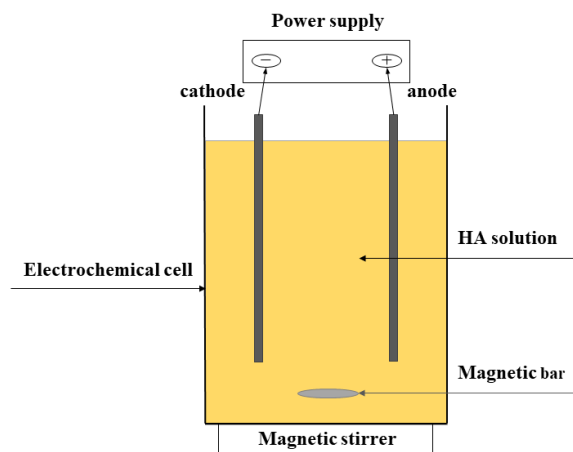

Figure 1. Diagrammatic representation of the electrochemical reactor.

2.4. UV–Vis Analysis

The starting HA solutions and the aliquots collected at programmed time-intervals during the electro-removal treatment were analyzed by UV–Vis spectroscopy. The UV–Vis spectra were recorded in the range of 200–800 nm on a Lambda 40, spectrometer, optical path = 1.00 cm (Perkin Elmer, Waltham, MA, USA). Quantitative analysis was performed using an absorbance–concentration calibration curve at 320 nm (molar extinction coefficient = 0.01412 L cm^{-1} mg^{-1}). After each test, the electrodes were washed with a solution containing Na$_4$P$_2$O$_7$ and NaOH, and the rinsing solution was analyzed by UV–Vis spectroscopy to verify the occurrence of HA adsorbed on the electrode surface. In no case was HA detected in measurable amount.

2.5. Low-Pressure Size-Exclusion Chromatography (LP-SEC)

In selected experiments, low-pressure size-exclusion chromatography was performed in order to obtain information on the molecular weight distribution of HA and of reaction products, using a Bio-Gel P10 Gel medium with 1.5–20 kDa fractional range (Bio-Rad Laboratories, Hercules, CA, USA), in a column 30 cm in length and 2.5 cm in diameter, eluted with 0.1 mol L^{-1} NaHCO$_3$ at a flow rate of 2.0 mL h^{-1}. Vanillic acid was used in LP-SEC experiments as a reference for low molecular weight HA-like compounds.

2.6. Total Organic Carbon

The total organic carbon (TOC) was determined at the end of the EO runs using a TOC-L CSN carbon analyzer (Shimadzu, Kyoto, Japan). Samples were heated to 680 °C in an oxygen-rich environment in combustion tubes filled with a platinum catalyst. The carbon dioxide generated by oxidation was measured with an infrared gas analyzer.

2.7. Elemental Analysis

The C/H ratios in the starting HA solution and two HA solutions obtained by the addition of 0.01 mol L^{-1} NaCl or NaClO$_4$ were determined by elemental analysis before and after the electro-removal runs. To this purpose, the solutions were first subjected to LP-SEC. The eluted fractions were recovered, and the pH was brought to about 3 with a dilute HCl solution. This procedure was performed twice. Finally, the samples were dialyzed against water to eliminate the residues of NaHCO$_3$ (eluent phase of the LP-SEC), lyophilized and analyzed using a CHN628 elemental analyzer (Leco, St. Joseph, Michigan, USA).

3. Results and Discussion

3.1. Electro-Oxidation of HA

The EO of HA was investigated under several different operational conditions: about one hundred kinetic runs were carried out to evaluate the effect of changes in HA and salt concentrations, type of electrolyte and current density.

UV spectroscopy and TOC measurements demonstrated a marked reduction of HA concentration in all experiments. During EO experiments, the release of bubbles from the electrodes was observed. According to the literature [66], this was probably due to the electrolysis of water leading to the formation of O$_2$ (anode) and H$_2$ (cathode) and causing overpotential phenomena. Figure 2 shows, as an example, the time dependence of HA concentration in two kinetic runs performed in the presence of 10 mM NaCl and 10 mM NaClO$_4$, respectively. The degradation reaction was faster for the sample containing NaCl. As discussed in detail in Section 3.2, the different degradation rates of HA in the presence of Cl$^-$ (reactive) and ClO$_4^-$ (inert) can be ascribed to the different chemical behavior of these anions under current flow.
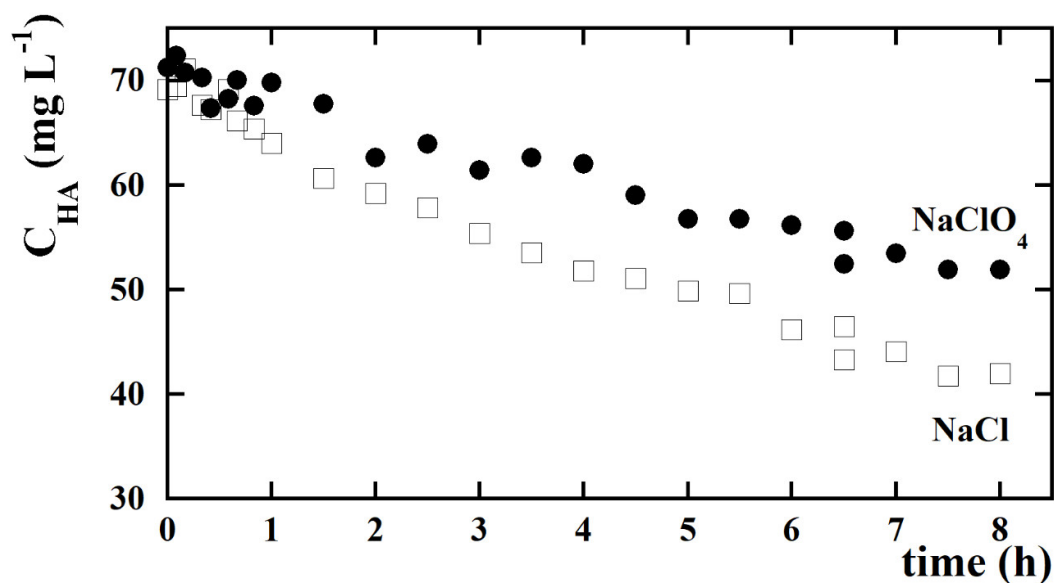

Figure 2. Effect of Cl$^-$ and ClO$_4^-$ anions on HA electro-oxidation: C_{HA} = 70mg L^{-1}, NaCl = 10 mM, NaClO$_4$ = 10 mM, initial pH =10.0, I = 115 Am^{-2}.

To explore the effect of each investigated parameter on the rate of HA oxidation, the initial reaction rates (v_0) of the experimental kinetic curves were estimated and compared. The values of v_0 (accessible in Supplementary Material) were obtained from the slope of the tangent to the concentration-time curve at $t = 0$. Figure 3 reports the full set of estimated v_0 values as a function of NaCl concentration at four current densities.
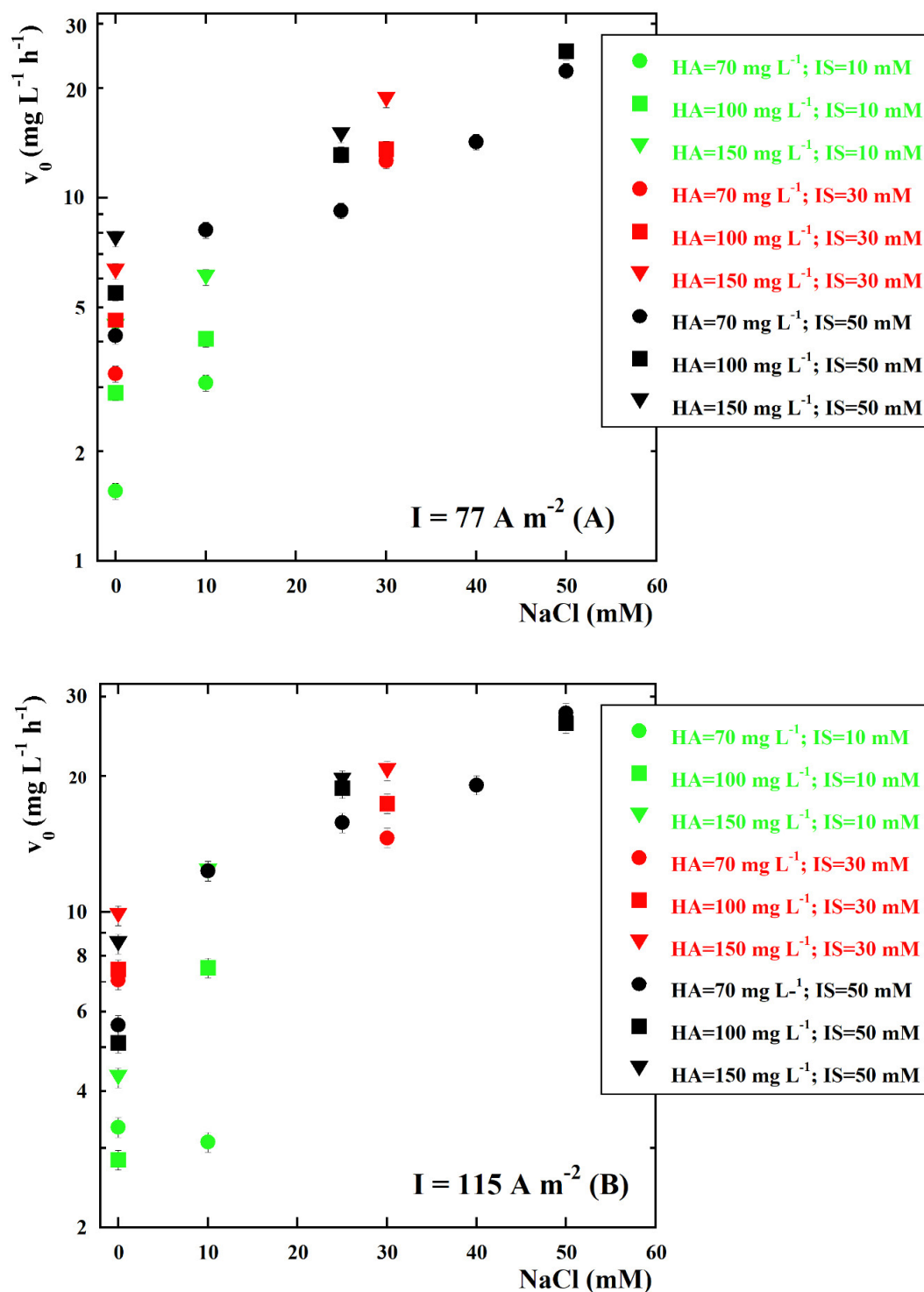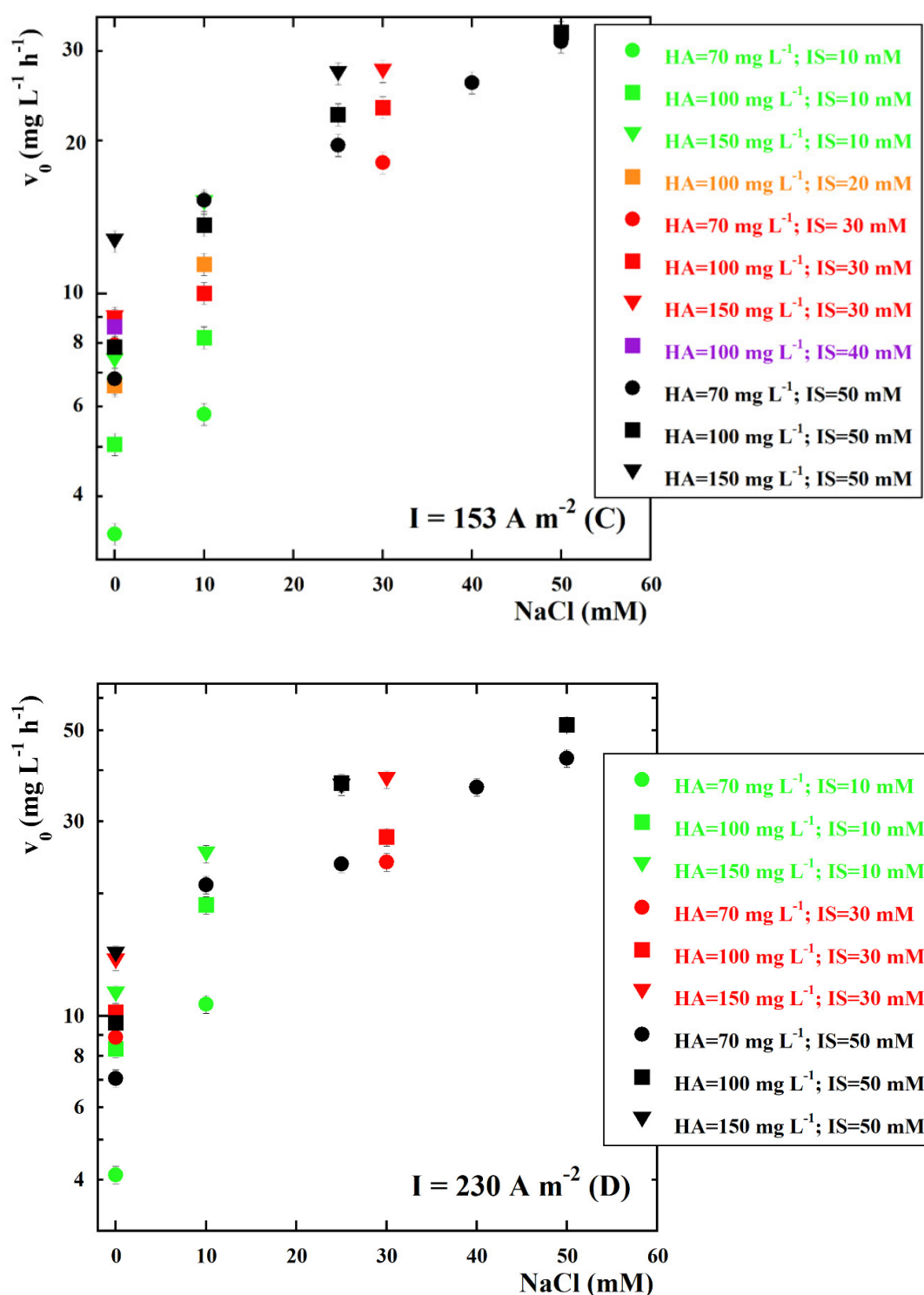

Figure 3. *Cont.*

Figure 3. Dependence of the initial reaction rate (v_0), on log scale, on NaCl concentration under different operational conditions: C_{HA} = 70–150 mg L^{-1}; NaClO$_4$ and NaNO$_3$ = 0–50 mM; *IS* = 10–50 mM; initial pH = 10.0; *I* = 77 A m^{-2} (**A**), 115 A m^{-2} (**B**), 153 A m^{-2} (**C**), 230 A m^{-2} (**D**).

As can be seen, the degradation rate was simultaneously affected by HA concentration, Cl$^-$ concentration, current density and ionic strength.

To clarify the role of HA concentration in the kinetics of the process, we investigated the dependence of v_0 on HA concentration for different current densities, while keeping the salt concentration constant. The results from experiments carried out in the presence of 10 mM NaClO$_4$ and 10 mM NaCl are

illustrated in Figure 4A,B, respectively. The curves were obtained by fitting the data to linear equations passing through the origin.
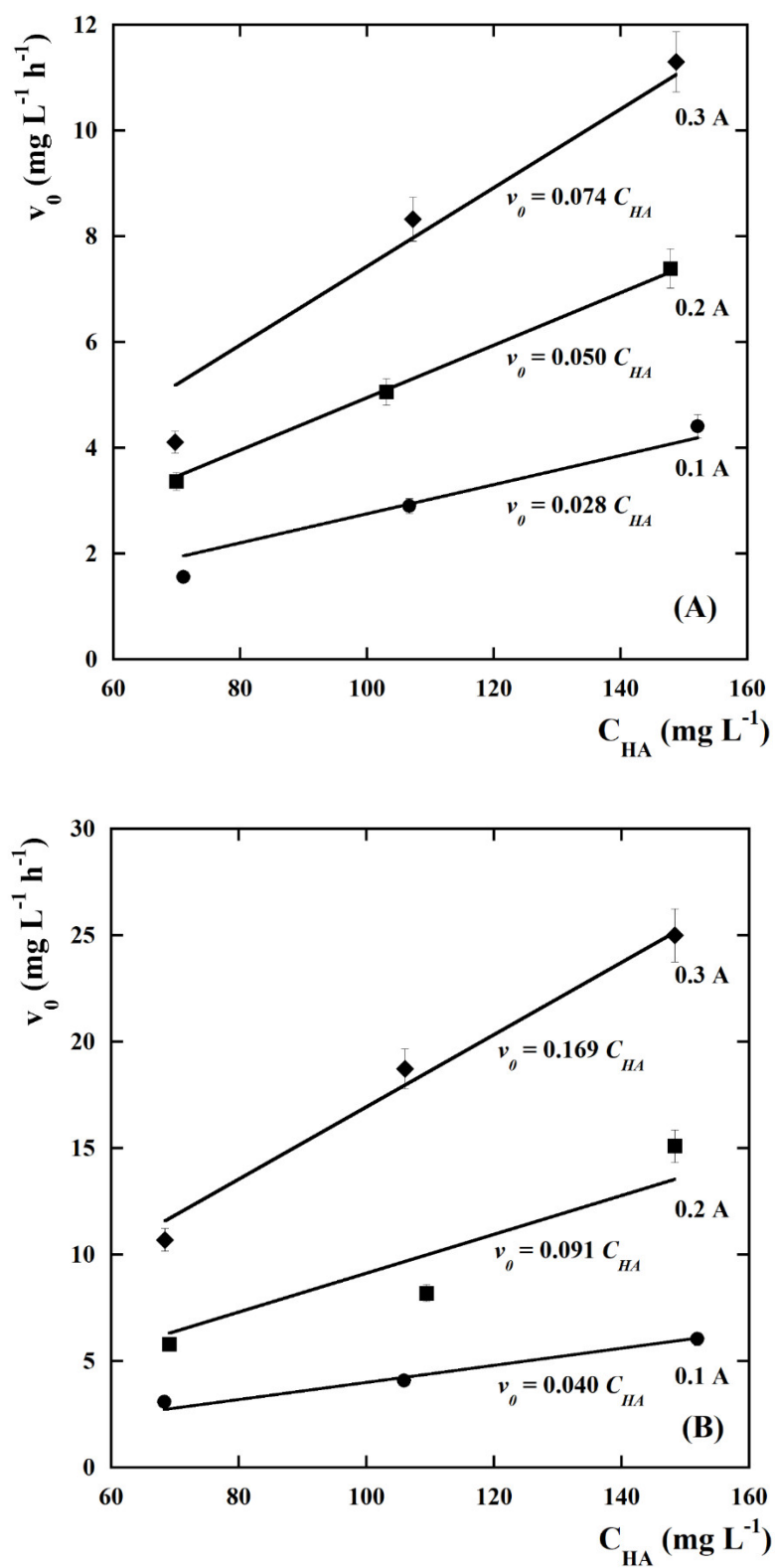

Figure 4. Dependence of the initial rate (v_0) of HA electro-oxidation as a function of C_{HA}, at different current densities; (**A**) 10 mM NaClO$_4$, (**B**) 10 mM NaCl.

The reaction rate linearly increased with increasing HA concentration, within experimental error, thus suggesting that the reaction obeys the first-order kinetics relative to HA. As clearly shown in Figure 4A,B, the slope of the lines proportionally increased with increasing current density. This suggests that the fraction of current loss due to undesirable side-reactions, such as the evolution of O_2 at the platinum anode [67], did not appreciably vary over the investigated range of current density.

The effect of ionic strength on the kinetics of HA EO was studied using $NaClO_4$ as an inert supporting electrolyte. Interestingly, an increase of the HA removal rate with increasing $NaClO_4$ concentration for all the investigated experimental conditions was observed (see Figure 5A). It is worth noting that the removal of HA was not strictly proportional to the salt concentration: the initial rate of HA oxidation increased less rapidly with respect to the increase of $NaClO_4$ (concave downward trend), as can be inferred from the slope of the lines in Figure 5A and from the data points in Figure 5B, which do not lie along a straight line passing from the origin. Experiments with another inert electrolyte, $NaNO_3$, gave similar results (see Table S1 in the Supplementary Materials). A similar, although less marked, effect of ionic strength on the oxidation rate of HA was also observed in the presence of chloride ions. Figure 5C shows, as an example, that the rate of HA EO in the presence of 10 mM Cl^- slightly increased with an increase in $NaClO_4$ concentration from 0 to 40 mM.
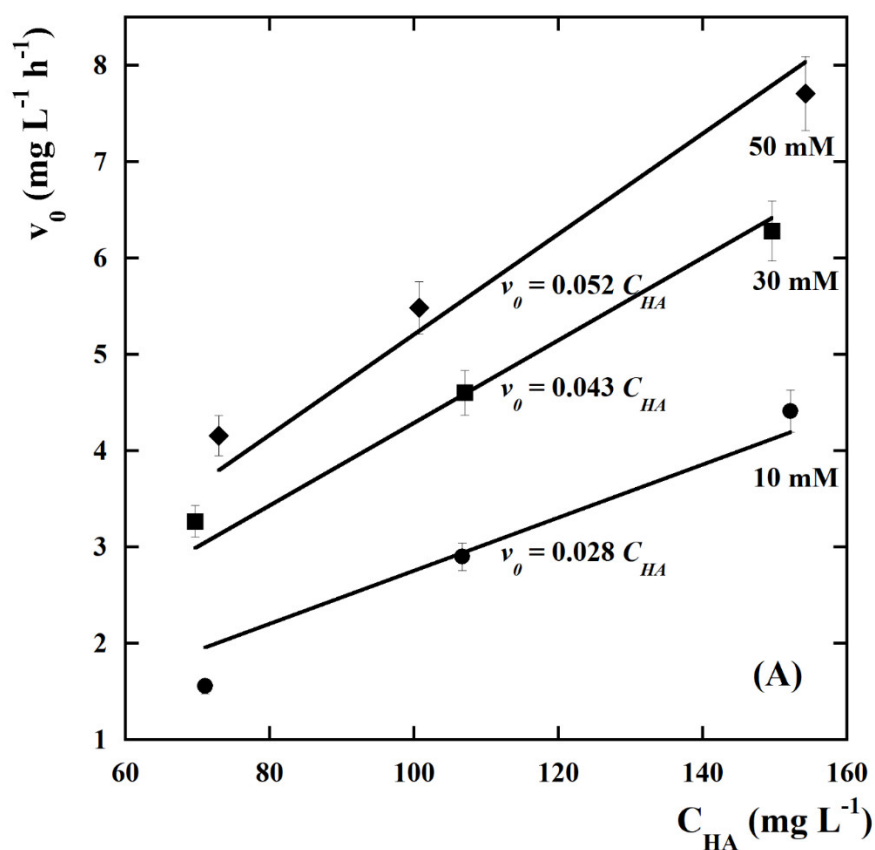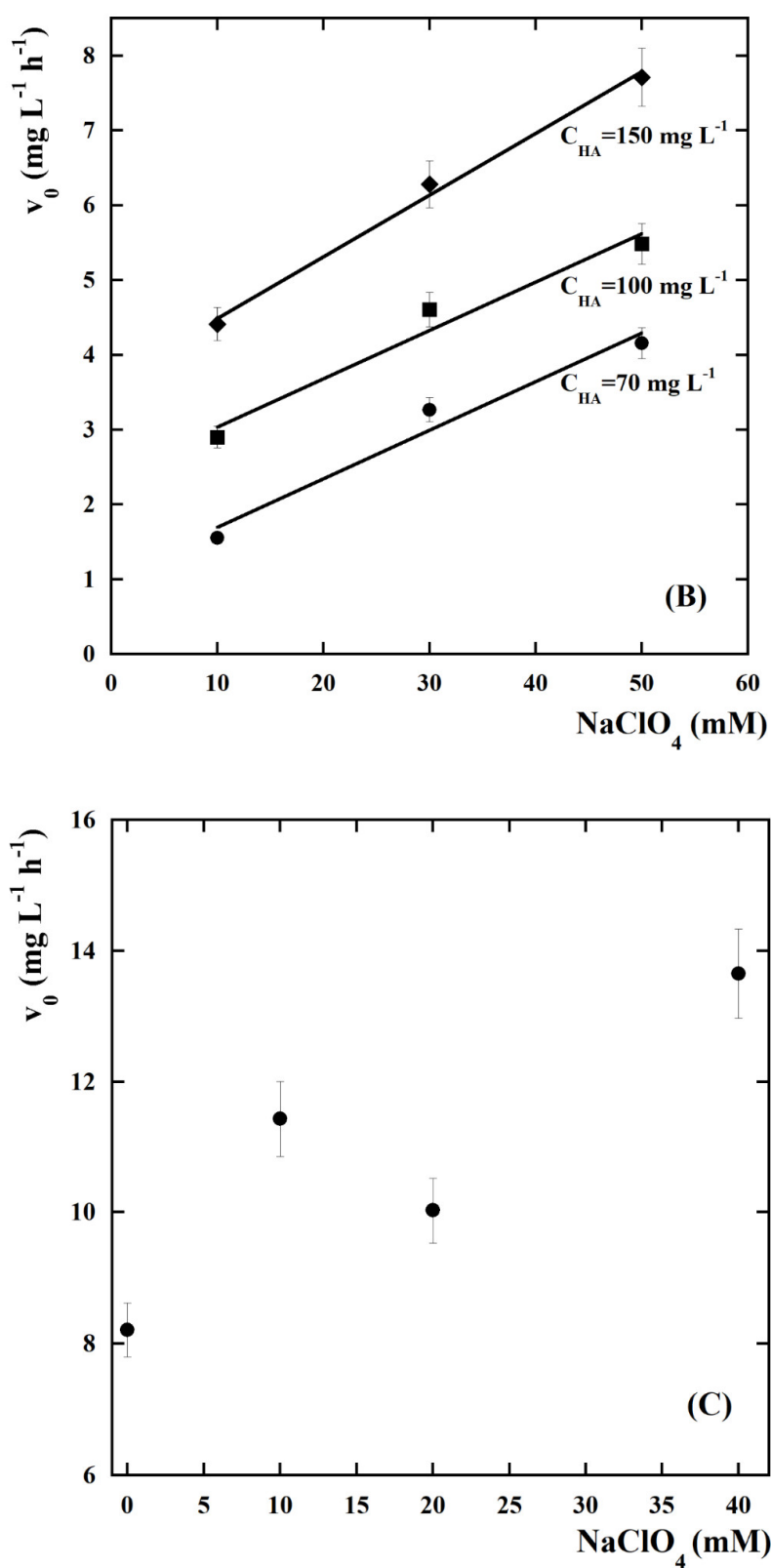

Figure 5. *Cont.*

Figure 5. Effect of the supporting inert electrolyte ($NaClO_4$) on the initial rate of HA electro-oxidation (v_0): (**A**) dependence of v_0 on C_{HA} at different $NaClO_4$ concentrations (10–50 mM), I = 77 A m^{-2}; (**B**) dependence of v_0 on $NaClO_4$ concentration at different C_{HA} (70–150 mg L^{-1}), I = 77 A m^{-2}; (**C**) effect of $NaClO_4$ concentration on v_0 in the presence of 10 mM NaCl, C_{HA} = 100 mg L^{-1}, I = 153 A m^{-2}.

The results presented above indicate that ionic strength plays an active role in HA EO. In line with transition state theory [68], a possible explanation for this behavior might be in the polyanionic nature of HA. Moreover, a rise in ionic strength causes HA molecules to shift to a more compact conformation, possibly altering their sensitivity to EO [69,70].

UV–Vis spectral analysis, TOC measurement, size-exclusion chromatography and elemental analysis provided useful information concerning the nature of the chemical species generated by the EO process. Figure 6 reports the UV–Vis spectra of untreated HA solution and of two HA solutions containing NaCl or NaClO₄ after the EO treatment.
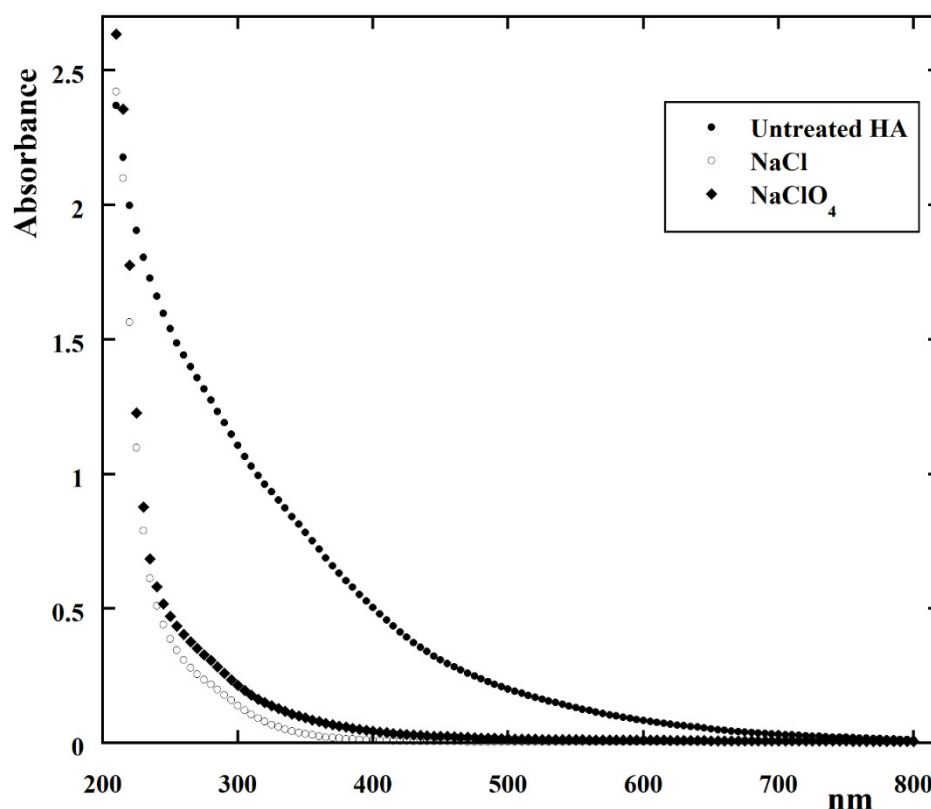

Figure 6. UV–Vis spectra of untreated HA containing 10 mM NaCl and after electrochemical treatment in the presence of 10mM NaCl and 10mM NaClO₄; I = 115 A m⁻². The UV–Vis spectrum of the untreated HA in the presences of 10 mM NaClO₄ is not shown because very similar to that of the untreated HA sample containing NaCl.

The spectrum of the untreated HA solution shows the typical HA absorbance in the UV–Vis region, reflecting the presence of conjugated double bonds systems and aromatic groups [71]. The spectra show a hypsochromic shift and a concomitant hypochromic effect in both treated solutions. These spectroscopic effects can only in part be ascribed to HA mineralization, in line with TOC reduction from 58.2 mg L^{-1} to 38.0 ($\approx$35% TOC reduction) and 29.0 mg L^{-1} ($\approx$50% TOC reduction) in the NaClO₄ and NaCl solution, respectively.

Figure 7 reports LP-SEC chromatograms of HA solution containing 10 mM NaCl, before and after EO and, for comparison, of vanillic acid (a low-molecular-weight HA-like compound). At the end of the EO experiment, the solution shows a reaction product with an intermediate retention time between the pristine HA sample and vanillic acid. This suggests that the treatment induces the formation of compounds with lower hydrodynamic volume (i.e., the volume of the molecules in solution) and lower molecular weight than the original HA molecules, while still retaining a macromolecular character. These findings are supported by dialysis experiments, which showed that the product of HA EO did not diffuse across a membrane with a relatively high cut off (6–8 kDa).
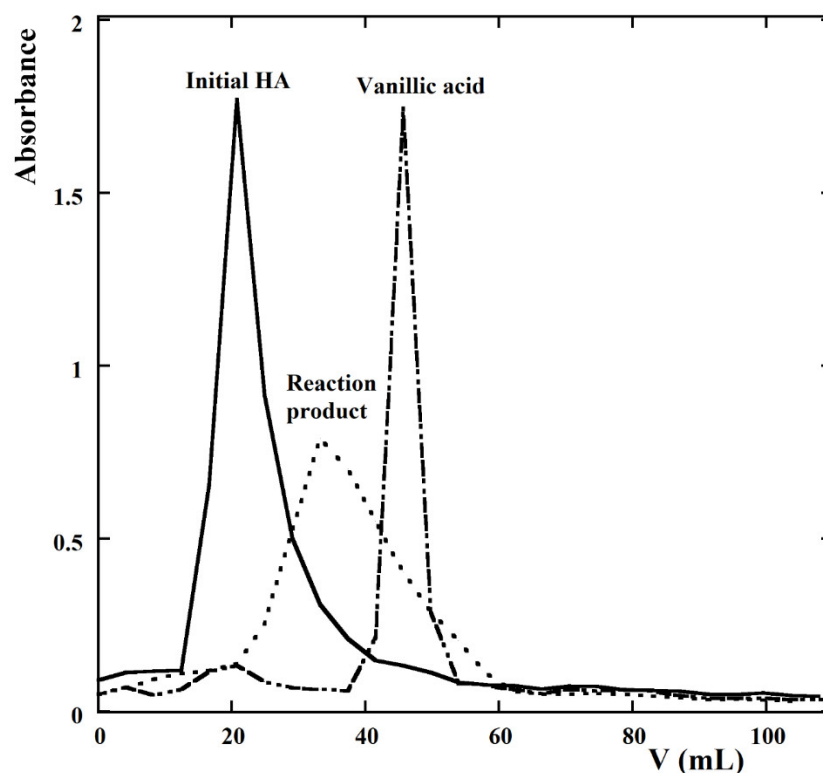
Figure 7. Low-pressure size exclusion chromatograms of untreated HA solution, of treated HA solution (reaction product) and, for comparison, of vanillic acid; NaCl concentration = 10 mM.

Elemental analysis showed that the C/H ratio decreased from 12.4 in the untreated solution to 9.0 and 8.5 in treated solutions containing $NaClO_4$ and NaCl, respectively. This suggests that the reaction product had a lower degree of unsaturation than the initial *HA*.

The full characterization and identification of byproducts was not possible. However, the formation of chlorinated compounds has been observed by several authors [72,73].

The TOC reduction obtained in the present work is quite low compared to that reported in other studies on HA EO, the main reason probably being passivation and high overpotential of platinum electrodes [66]. Alternative electrode materials may strongly enhance the dispersion of anions in the solution and, therefore, the removal of HA [74–76]. Better HA aqueous removal efficiency was obtained, for example, by Deng et al. [49] using a Ti/RuO_2 anode, an electric current density of 100 mA/cm^2 and pH 6.5. Those authors observed a reduction of chemical oxygen demand (COD) by over 80% in biologically pre-treated landfill leachate. Wang et al. [10] reported complete mineralization of HA from an effluent of biotreated coking wastewater after 30-min treatment involving boron-doped diamond anodes. Trellu et al. [59] obtained nearly 99% reduction of TOC in drinking water within 7-h treatment at 1000 mA, using a boron doped diamond anode and a stainless-steel cathode.

3.2. Kinetic Modelling

In line with former work [60], the experimental data reported above suggest that the degradation of HA may proceed through one or two pathways, depending on whether chloride is present or not.

In the presence of inert supporting electrolytes (in our protocol, $NaClO_4$ or $NaNO_3$) but without chlorides (or of other salts, such as sulfates, from which oxidant species can be electro-generated), HA EO only depends on the formation of hydroxyl radicals by water discharge at the anode [52]. The first step of this oxidative pathway is water interaction with active sites at the anode surface leading to the formation of adsorbed hydroxyl radicals (Equation (1)):
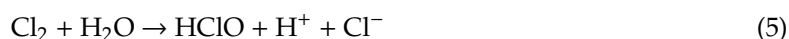
$$H_2O + Pt \rightarrow Pt(OH^\bullet) + H^+ + e^- \tag{1}$$
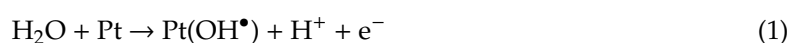
In the second step, hydroxyl radicals oxidize HA (Equation (2)):

$$Pt(OH^\bullet) + HA \rightarrow Pt + Oxidized\ HA \tag{2}$$

Oxidation can only occur in close proximity to the anode, because hydroxyl radicals have a very short lifetime [52]. Thus, the rate of reaction (2) most likely controls the overall reaction rate. If so, HA concentration should be a primary determinant of the reaction rate. Our experimental results support this conclusion by showing a linear relationship between the reaction rate and HA concentration (Figure 4A).

The rate of HA degradation in the presence of NaCl as electrolyte was significantly higher than with $NaClO_4$ or $NaNO_3$ (Figures 2 and 4), indicating that HA oxidation not only occurred via hydroxyl radicals, as was the case with inert electrolytes, but additionally involving active chlorine species originating from chloride ions during the electrochemical process. Active chlorine species such as Cl_2, $HClO$ and ClO^- may be generated at the anode by the following reactions [52]:

$$2Cl^- \rightarrow 2Cl^\bullet + 2e^- \tag{3}$$

$$2Cl^\bullet \rightarrow Cl_2 \tag{4}$$

$$Cl_2 + H_2O \rightarrow HClO + H^+ + Cl^- \tag{5}$$

$$HClO \leftrightarrow H^+ + ClO^- \tag{6}$$

Although active chlorine species have lower reduction potentials than hydroxyl radicals, they may be more efficient oxidants because, after formation at the anode, they are sufficiently stable to diffuse into the solution and bulk-react with HA. The relative abundance of Cl_2, $HClO$ and ClO^- depends on pH. At pH 10 chosen for our experiments, ClO^- dominates over the other species and is probably the main driver of HA EO [77].

The reactions of HA oxidation by hydroxyl radicals and active chlorine species probably proceed in parallel as sketched in Figure 8, with k_{OH} and k_{Cl} being the kinetic rate constants of either pathway.
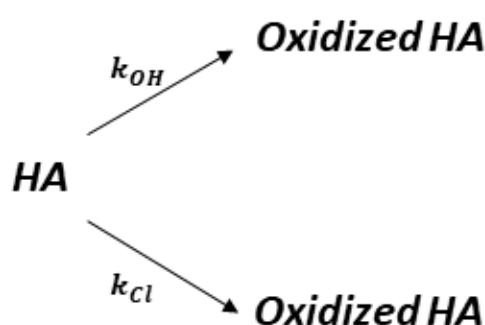

Figure 8. Proposed pathways for the electro-oxidation of *HA*.

In order to model the kinetics of HA degradation, we used the initial reaction rate method, a method widely used in enzymatic kinetics [78]. This approach has the advantage of being independent of the time evolution of reactive species and operational conditions (e.g., HA, pH, concentration of chlorine species and $OH^\bullet$).

Based on the above reasoning and in line with the data presented, we propose the following equation to describe the initial rate of HA EO in the presence of inert supporting electrolytes ($v_{0,OH}$, upper reaction pathway in Figure 8):

$$v_{0,OH} = -(dC_{HA}/dt)_0 = k_{OH} \times C_{HA} \times IS^n \times I \tag{7}$$

where C_{HA}, IS and I are the initial HA concentration, ionic strength and current density, respectively, and n is a constant.

The rate of HA EO in the presence of Cl^- (lower reaction pathway in Figure 8) depends on the formation rate of both hydroxyl radicals and active chlorine species. In line with our experimental data, the initial rate of HA electro-oxidation in the presence of Cl^- ($v_{0,Cl}$) varies with the initial chloride concentration (C_{Cl^-}), C_{HA}, IS and I according to the following relation:

$$v_{0,Cl} = -(dC_{HA}/dt)_0 = k_{Cl} \times C_{Cl^-} \times C_{HA} \times IS^n \times I \tag{8}$$

The quantity IS^n in Equations (7) and (8) was introduced to take into account the observed effect of ionic strength, which unlike C_{HA}, C_{Cl^-} and I cannot be described by a first-kinetic-order reaction (cf. Figure 5).

The overall initial rate (v_0) of HA electro-oxidation can be obtained by summing up Equations (7) and (8):

$$v_0 = k_{OH} \times C_{HA} \times IS^n \times I + k_{Cl} \times C_{Cl^-} \times C_{HA} \times IS^n \times I \tag{9}$$

To test the validity of the above model and estimate the kinetic parameters, the initial reaction rate (v_0) values shown in Figure 3 were fitted to Equation (9) using a multivariable fitting procedure (Table 1).

Table 1. Kinetic parameters for the *EO* of *HA*.

k_{Cl} ($\mathbf{L^{n+1}\ m^2\ mmol^{-(n+1)}h^{-1}\ A^{-1}}$)	k_{OH} ($\mathbf{L^n\ m^2\ mmol^{-n}h^{-1}\ A^{-1}}$)	n	Adjusted R^2
$(1.4 \pm 0.3) \times 10^{-5}$	$(2.0 \pm 0.4) \times 10^{-4}$	0.24 ± 0.06	0.93

Our kinetic model fitted the experimental data well (as shown by a high adjusted R^2 value) and produced a reliable estimation of kinetic parameters (because of relatively low associated standard errors). As expected, the results point to a significant effect of ionic strength ($n = 0.24$). Noticeably, the values of the estimated kinetic parameters suggest that, at low Cl^- concentration (e.g., 10 mM), the rate of the oxidation of HA is mainly promoted by the hydroxyl radicals, i.e., the pathway mediated by hydroxyl radicals predominates over the pathway depending on active chlorine species.

The accuracy of the above model was verified by parity plotting model predictions and experimentally measured values of initial v_0 (Figure 9). Most points fell in a variation range of ±30%, indicating a satisfactory agreement between predicted and experimental data for all operative conditions tested. This supports our kinetic model as a reliable description of HA EO in the experimental conditions investigated.
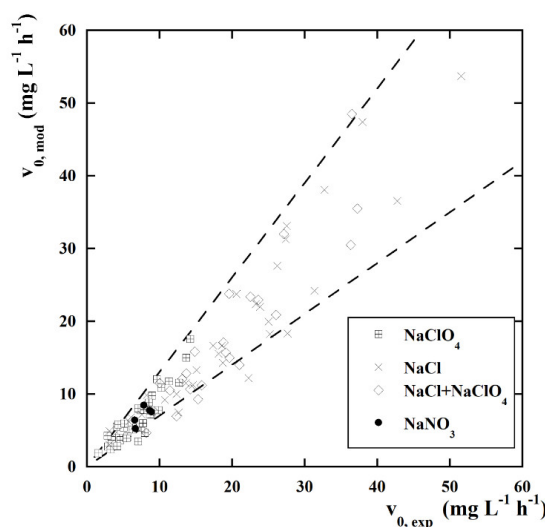

Figure 9. Parity plot (±30%) of predicted vs. experimentally determined initial reaction rates of HA electro-oxidation under different operational conditions.

4. Conclusions

The electro-treatment of HA solution using Pt electrodes led to rapid oxidation of HA into smaller molecules with lower aromaticity and conjugation degree. The impacts of these products on the ecosystem and human health remain to be determined. Humic acids EO may proceed through two concurrent reactions, one mediated by reactive chlorine species, the other by hydroxyl radicals, the latter being dominant at low chlorine concentration. Kinetic analysis suggests that the overall reaction rate is of a first-order relative to HA and Cl^- concentrations and current density. An appreciable effect of ionic strength was observed, probably due to the polyanionic nature of HA molecules. A kinetic model was proposed and successfully applied to predict the rate of HA electro-oxidation.

References

1. Richardson, S.D.; Ternes, T.A. Water Analysis: Emerging Contaminants and Current Issues. *Anal. Chem.* **2018**, *90*, 398–428. [CrossRef] [PubMed]
2. Erto, A.; Andreozzi, R.; Di Natale, F.; Lancia, A.; Musmarra, D. Experimental and isotherm-models analysis on TCE and PCE adsorption onto activated carbon. *Chem. Eng. Trans.* **2009**, *17*, 293–298. [CrossRef]
3. Colella, A.; de Gennaro, B.; Salvestrini, S.; Colella, C. Surface interaction of humic acids with natural and synthetic phillipsite. *J. Porous Mater.* **2015**, *22*, 501–509. [CrossRef]
4. Jones, M.N.; Bryan, N.D. Colloidal properties of humic substances. *Adv. Colloid Interface Sci.* **1998**, *78*, 1–48. [CrossRef]
5. Chianese, S.; Fenti, A.; Iovino, P.; Musmarra, D.; Salvestrini, S. Sorption of organic pollutants by humic acids: A review. *Molecules* **2020**, *25*, 918. [CrossRef] [PubMed]
6. Fernandes, A.; Pacheco, M.J.; Ciríaco, L.; Lopes, A. Review on the electrochemical processes for the treatment of sanitary landfill leachates: Present and future. *Appl. Catal. B Environ.* **2015**, *176*, 183–200. [CrossRef]
7. Renou, S.; Givaudan, J.G.; Poulain, S.; Dirassouyan, F.; Moulin, P. Landfill leachate treatment: Review and opportunity. *J. HAzard. Mater.* **2008**, *150*, 468–493. [CrossRef]
8. Schellekens, J.; Buurman, P.; Kalbitz, K.; Van Zomeren, A.; Vidal-Torrado, P.; Cerli, C.; Comans, R.N.J. Molecular Features of Humic Acids and Fulvic Acids from Contrasting Environments. *Environ. Sci. Technol.* **2017**, *51*, 1330–1339. [CrossRef]
9. Zhang, G.; Lee, D.J.; Cheng, F. Treatment of domestic sewage with anoxic/oxic membrane-less microbial fuel cell with intermittent aeration. *Bioresour. Technol.* **2016**, *218*, 680–686. [CrossRef]
10. Wang, C.; Zhang, M.; Liu, W.; Ye, M.; Su, F. Effluent characteristics of advanced treatment for biotreated coking wastewater by electrochemical technology using BDD anodes. *Environ. Sci. Pollut. Res.* **2015**, *22*, 6827–6834. [CrossRef]
11. Cowman, G.A.; Singer, P.C. Effect of bromide ion on haloacetic acid speciation resulting from chlorination and chloramination of aquatic humic substances. *Environ. Sci. Technol.* **1996**, *30*, 16–24. [CrossRef]
12. Iovino, P.; Leone, V.; Salvestrini, S.; Capasso, S. Sorption of non-ionic organic pollutants onto immobilized humic acid. *Desalin. Water Treat.* **2015**, *56*, 55–62. [CrossRef]
13. Lin, J.; Zhan, Y. Adsorption of humic acid from aqueous solution onto unmodified and surfactant-modified chitosan/zeolite composites. *Chem. Eng. J.* **2012**, *200*, 202–213. [CrossRef]
14. Wu, Y.; Zhou, S.; Ye, X.; Zhao, R.; Chen, D. Oxidation and coagulation removal of humic acid using Fenton process. *Colloids Surf. A Physicochem. Eng. Asp.* **2011**, *379*, 151–156. [CrossRef]

15. Liu, J.; Cao, J.; Chen, H.; Zhou, D. Adsorptive removal of humic acid from aqueous solution by micro- and mesoporous covalent triazine-based framework. *Colloids Surf. A Physicochem. Eng. Asp.* **2015**, *481*, 276–282. [CrossRef]

16. Salvestrini, S. Diuron herbicide degradation catalyzed by low molecular weight humic acid-like compounds. *Environ. Chem. Lett.* **2013**, *11*, 359–363. [CrossRef]

17. Wang, H.; Zhang, J.; Yuan, X.; Jiang, L.; Xia, Q.; Chen, H. Photocatalytic removal of antibiotics from natural water matrices and swine wastewater via Cu(I) coordinately polymeric carbon nitride framework. *Chem. Eng. J.* **2020**, *392*, 123638. [CrossRef]

18. Muhammad, A.; Shah, A.H.A.; Bilal, S. Effective Adsorption of Hexavalent Chromium and Divalent Nickel Ions from Water through Polyaniline, Iron Oxide, and Their Composites. *Appl. Sci.* **2020**, *10*, 2882. [CrossRef]

19. Kamel, R.M.; Shahat, A.; Hegazy, W.H.; Khodier, E.M.; Awual, M.R. Efficient toxic nitrite monitoring and removal from aqueous media with ligand based conjugate materials. *J. Mol. Liq.* **2019**, *285*, 20–26. [CrossRef]

20. Awual, M.R.; Hasan, M.M.; Iqbal, J.; Islam, M.A.; Islam, A.; Khandaker, S.; Asiri, A.M.; Rahman, M.M. Ligand based sustainable composite material for sensitive nickel(II) capturing in aqueous media. *J. Environ. Chem. Eng.* **2020**, *8*, 103591. [CrossRef]

21. Salvestrini, S. A modification of the Langmuir rate equation for diffusion-controlled adsorption kinetics. *React. Kinet. Mech. Catal.* **2019**, *128*, 571–586. [CrossRef]

22. Leone, V.; Iovino, P.; Canzano, S.; Salvestrini, S.; Capasso, S. Water purification from humic acids by clinoptilolite-rich tuff. *Environ. Eng. Manag. J.* **2013**, *12*, 3–6.

23. Salvestrini, S.; Jovanović, J.; Adnadjević, B. Comparison of adsorbent materials for herbicide diuron removal from water. *Desalin. Water Treat.* **2016**, *57*, 22868–22877. [CrossRef]

24. Salvestrini, S.; Vanore, P.; Iovino, P.; Leone, V.; Capasso, S. Adsorption of simazine and boscalid onto acid-activated natural clinoptilolite. *Environ. Eng. Manag. J.* **2015**, *14*, 1705–1712. [CrossRef]

25. Lingamdinne, L.P.; Vemula, K.R.; Chang, Y.Y.; Yang, J.K.; Karri, R.R.; Koduru, J.R. Process optimization and modeling of lead removal using iron oxide nanocomposites generated from bio-waste mass. *Chemosphere* **2020**, *243*, 125257. [CrossRef] [PubMed]

26. Spaltro, A.; Simonetti, S.; Laurella, S.; Ruiz, D.; Compañy, A.D.; Juan, A.; Allegretti, P. Adsorption of bentazone and imazapyc from water by using functionalized silica: Experimental and computational analysis. *J. Contam. Hydrol.* **2019**, *227*, 103542. [CrossRef]

27. Czepa, W.; Pakulski, D.; Witomska, S.; Patroniak, V.; Ciesielski, A.; Samorì, P. Graphene oxide-mesoporous SiO2 hybrid composite for fast and efficient removal of organic cationic contaminants. *Carbon* **2020**, *158*, 193–201. [CrossRef]

28. Yu, S.; Wang, J.; Cui, J. Preparation of a novel chitosan-based magnetic adsorbent CTS@SnO2@Fe3O4 for effective treatment of dye wastewater. *Int. J. Biol. Macromol.* **2019**. [CrossRef]

29. Canzano, S.; Capasso, S.; Di Natale, M.; Erto, A.; Iovino, P.; Musmarra, D. Remediation of groundwater polluted by aromatic compounds by means of adsorption. *Sustainability* **2014**, *6*, 4807–4822. [CrossRef]

30. Erto, A.; Chianese, S.; Lancia, A.; Musmarra, D. On the mechanism of benzene and toluene adsorption in single-compound and binary systems: Energetic interactions and competitive effects. *Desalin. Water Treat.* **2017**, *86*, 259–265. [CrossRef]

31. Salvestrini, S.; Vanore, P.; Bogush, A.; Mayadevi, S.; Campos, L.C. Sorption of metaldehyde using granular activated carbon. *J. Water Reuse Desalin.* **2017**, *7*, 280–287. [CrossRef]

32. Chu, L.; Zhang, J.; Wu, Z.; Wang, C.; Sun, Y.; Dong, S.; Sun, J. Solar-driven photocatalytic removal of organic pollutants over direct Z-scheme coral-branch shape Bi2O3/SnO2 composites. *Mater. CHAract.* **2020**, *159*, 110036. [CrossRef]

33. Iovino, P.; Chianese, S.; Prisciandaro, M.; Musmarra, D. Triclosan photolysis: Operating condition study and photo-oxidation pathway. *Chem. Eng. J.* **2019**, *377*. [CrossRef]

34. Iovino, P.; Chianese, S.; Canzano, S.; Prisciandaro, M.; Musmarra, D. Ibuprofen photodegradation in aqueous solutions. *Environ. Sci. Pollut. Res.* **2016**, *23*, 22993–23004. [CrossRef] [PubMed]

35. Chianese, S.; Iovino, P.; Canzano, S.; Prisciandaro, M.; Musmarra, D. Ibuprofen degradation in aqueous solution by using UV light. *Desalin. Water Treat.* **2016**, *57*, 22878–22886. [CrossRef]

36. Bensalah, N.; Ahmad, M.I.; Bedoui, A. Catalytic degradation of 4-ethylpyridine in water by heterogeneous photo-fenton process. *Appl. Sci.* **2019**, *9*, 5073. [CrossRef]

37. Musmarra, D.; Prisciandaro, M.; Capocelli, M.; Karatza, D.; Iovino, P.; Canzano, S.; Lancia, A. Degradation of ibuprofen by hydrodynamic cavitation: Reaction pathways and effect of operational parameters. *Ultrason. Sonochem.* **2016**, *29*, 76–83. [CrossRef]

38. Dong, Z.Y.; Zhang, K.; Yao, R.H. Degradation of refractory pollutants by hydrodynamic cavitation: Key parameters to degradation rates. *J. Hydrodyn.* **2019**, *31*, 848–856. [CrossRef]

39. Murray, C.A.; Parsons, S.A. Advanced oxidation processes: Flowsheet options for bulk natural organic matter removal. *Water Sci. Technol. Water Supply* **2004**, *4*, 113–119. [CrossRef]

40. Silva, A.C.; Dezotti, M.; Sant'Anna, G.L. Treatment and detoxification of a sanitary landfill leachate. *Chemosphere* **2004**, *55*, 207–214. [CrossRef]

41. Beltrán, F.J.; Rivas, F.J.; Gimeno, O. Comparison between photocatalytic ozonation and other oxidation processes for the removal of phenols from water. *J. Chem. Technol. Biotechnol.* **2005**, *80*, 973–984. [CrossRef]

42. Zambrano, J.; Park, H.; Min, B. Enhancing electrochemical degradation of phenol at optimum pH condition with a Pt/Ti anode electrode. *Environ. Technol.* **2019**. [CrossRef] [PubMed]

43. Sopaj, F.; Rodrigo, M.A.; Oturan, N.; Podvorica, F.I.; Pinson, J.; Oturan, M.A. Influence of the anode materials on the electrochemical oxidation efficiency. Application to oxidative degradation of the pharmaceutical amoxicillin. *Chem. Eng. J.* **2015**, *262*, 286–294. [CrossRef]

44. Särkkä, H.; Bhatnagar, A.; Sillanpää, M. Recent developments of electro-oxidation in water treatment—A review. *J. Electroanal. Chem.* **2015**, *754*, 46–56. [CrossRef]

45. Qin, Y.; Cui, Y.; Lei, L.; Gao, Y.; Zhou, Z.; Li, Y.; Shi, X. An Electrochemical Process Comparison of As(III) in Simulated Groundwater at Low Voltage in Mixed and Divided Electrolytic Cells. *Water* **2020**, *12*, 1126. [CrossRef]

46. Dao, K.C.; Yang, C.-C.; Chen, K.-F.; Tsai, Y.-P. Recent Trends in Removal Pharmaceuticals and Personal Care Products by Electrochemical Oxidation and Combined Systems. *Water* **2020**, *12*, 1043. [CrossRef]

47. Martínez-Huitle, C.A.; Ferro, S. Electrochemical oxidation of organic pollutants for the wastewater treatment: Direct and indirect processes. *Chem. Soc. Rev.* **2006**, *35*, 1324–1340. [CrossRef]

48. Mandal, P.; Dubey, B.K.; Gupta, A.K. Review on landfill leachate treatment by electrochemical oxidation: Drawbacks, challenges and future scope. *Waste Manag.* **2017**, *69*, 250–273. [CrossRef]

49. Deng, Y.; Chen, N.; Feng, C.; Chen, F.; Wang, H.; Kuang, P.; Feng, Z.; Liu, T.; Gao, Y.; Hu, W. Treatment of organic wastewater containing nitrogen and chlorine by combinatorial electrochemical system: Taking biologically treated landfill leachate treatment as an example. *Chem. Eng. J.* **2019**, *364*, 349–360. [CrossRef]

50. Baddouh, A.; Bessegato, G.G.; Rguiti, M.M.; El Ibrahimi, B.; Bazzi, L.; Hilali, M.; Zanoni, M.V.B. Electrochemical decolorization of Rhodamine B dye: Influence of anode material, chloride concentration and current density. *J. Environ. Chem. Eng.* **2018**, *6*, 2041–2047. [CrossRef]

51. Fernandes, A.; Santos, D.; Pacheco, M.J.; Ciríaco, L.; Lopes, A. Electrochemical oxidation of humic acid and sanitary landfill leachate: Influence of anode material, chloride concentration and current density. *Sci. Total Environ.* **2016**, *541*, 282–291. [CrossRef] [PubMed]

52. Serrano, K.G. Indirect electrochemical oxidation using hydroxyl radical, active chlorine, and peroxodisulfate. In *Electrochemical Water and Wastewater Treatment*; Elsevier: Amsterdam, The Netherlands, 2018; pp. 133–164. ISBN 9780128131602. [CrossRef]

53. Vagi, M.C.; Petsas, A.S. Recent advances on the removal of priority organochlorine and organophosphorus biorecalcitrant pesticides defied by Directive 2013/39/EU from environmental matrices by using advanced oxidation processes: An overview (2007–2018). *J. Environ. Chem. Eng.* **2019**, 102940. [CrossRef]

54. Zhu, X.; Ni, J.; Wei, J.; Xing, X.; Li, H. Destination of organic pollutants during electrochemical oxidation of biologically-pretreated dye wastewater using boron-doped diamond anode. *J. HAzard. Mater.* **2011**, *189*, 127–133. [CrossRef] [PubMed]

55. Berenguer, R.; Quijada, C.; La Rosa-Toro, A.; Morallón, E. Electro-oxidation of cyanide on active and non-active anodes: Designing the electrocatalytic response of cobalt spinels. *Sep. Purif. Technol.* **2019**, *208*, 42–50. [CrossRef]

56. Zhu, X.; Ni, J.; Lai, P. Advanced treatment of biologically pretreated coking wastewater by electrochemical oxidation using boron-doped diamond electrodes. *Water Res.* **2009**, *43*, 4347–4355. [CrossRef]

57. Cañizares, P.; Martínez, L.; Paz, R.; Sáez, C.; Lobato, J.; Rodrigo, M.A. Treatment of Fenton-refractory olive oil mill wastes by electrochemical oxidation with boron-doped diamond anodes. *J. Chem. Technol. Biotechnol.* **2006**, *81*, 1331–1337. [CrossRef]

58. Dbira, S.; Bensalah, N.; Ahmad, M.I.; Bedoui, A. Electrochemical oxidation/disinfection of urine wastewaters with different anode materials. *Materials* **2019**, *12*, 1254. [CrossRef]

59. Trellu, C.; Péchaud, Y.; Oturan, N.; Mousset, E.; Huguenot, D.; van Hullebusch, E.D.; Esposito, G.; Oturan, M.A. Comparative study on the removal of humic acids from drinking water by anodic oxidation and electro-Fenton processes: Mineralization efficiency and modelling. *Appl. Catal. B Environ.* **2016**, *194*, 32–41. [CrossRef]

60. Capasso, S.; Salvestrini, S.; Roviello, V.; Trifuoggi, M.; Iovino, P. Electrochemical removal of humic acids from water using aluminum anode: Influence of chloride ion and current parameters. *J. Chem.* **2019**, *2019*. [CrossRef]

61. Mahvi, A.H.; Bazrafshan, E.; Biglari, H. Humic acid removal from aqueous environments by electrocoagulation process using iron electrodes. *E J. Chem.* **2012**, *9*, 2453–2461. [CrossRef]

62. Leone, V.; Musmarra, D.; Iovino, P.; Capasso, S. Sorption Equilibrium of Aromatic Pollutants onto Dissolved Humic Acids. *Water. Air. Soil Pollut.* **2017**, *228*. [CrossRef]

63. Salvestrini, S. New insights into the interaction mechanism of humic acids with phillipsite. *React. Kinet. Mech. Catal.* **2017**, *120*, 735–752. [CrossRef]

64. Engebretson, R.R.; von Wandruszka, R. Microorganization in Dissolved Humic Acids. *Environ. Sci. Technol.* **1994**, *28*, 1934–1941. [CrossRef] [PubMed]

65. Guetzloff, T.F.; Rice, J.A. Does humic acid form a micelle? *Sci. Total Environ.* **1994**, *152*, 31–35. [CrossRef]

66. Mousset, E.; Dionysiou, D.D. Photoelectrochemical reactors for treatment of water and wastewater: A review. *Environ. Chem. Lett.* **2020**, *18*, 1301–1318. [CrossRef]

67. Zazou, H.; Oturan, N.; Zhang, H.; Hamdani, M.; Oturan, M.A. Comparative study of electrochemical oxidation of herbicide 2,4,5-T: Kinetics, parametric optimization and mineralization pathway. *Sustain. Environ. Res.* **2017**, *27*, 15–23. [CrossRef]

68. Seiffert, S.; Sprakel, J. Physical chemistry of supramolecular polymer networks. *Chem. Soc. Rev.* **2012**, *41*, 909–930. [CrossRef]

69. Baalousha, M.; Motelica-Heino, M.; Coustumer, P. Le Conformation and size of humic substances: Effects of major cation concentration and type, pH, salinity, and residence time. *Colloids Surf. A Physicochem. Eng. Asp.* **2006**, *272*, 48–55. [CrossRef]

70. Wang, L.F.; Wang, L.L.; Ye, X.D.; Li, W.W.; Ren, X.M.; Sheng, G.P.; Yu, H.Q.; Wang, X.K. Coagulation kinetics of humic aggregates in mono- and Di-valent electrolyte solutions. *Environ. Sci. Technol.* **2013**, *47*, 5042–5049. [CrossRef]

71. Rodig, O.R. *Spectrometric Identification of Organic Compounds*, 8th ed.; John Wiley & Sons Inc.: Hoboken, NJ, USA, 1963; Volume 6, ISBN 978-0470616376.

72. Anglada, Á.; Urtiaga, A.; Ortiz, I.; Mantzavinos, D.; Diamadopoulos, E. Boron-doped diamond anodic treatment of landfill leachate: Evaluation of operating variables and formation of oxidation by-products. *Water Res.* **2011**, *45*, 828–838. [CrossRef]

73. Pérez, G.; Saiz, J.; Ibañez, R.; Urtiaga, A.M.; Ortiz, I. Assessment of the formation of inorganic oxidation by-products during the electrocatalytic treatment of ammonium from landfill leachates. *Water Res.* **2012**, *46*, 2579–2590. [CrossRef] [PubMed]

74. Awual, M.R. Solid phase sensitive palladium(II) ions detection and recovery using ligand based efficient conjugate nanomaterials. *Chem. Eng. J.* **2016**, *300*, 264–272. [CrossRef]

75. Awual, M.R. New type mesoporous conjugate material for selective optical copper(II) ions monitoring & removal from polluted waters. *Chem. Eng. J.* **2017**, *307*, 85–94. [CrossRef]

76. Awual, M.R. Ring size dependent crown ether based mesoporous adsorbent for high cesium adsorption from wastewater. *Chem. Eng. J.* **2016**, *303*, 539–546. [CrossRef]

77. Cherney, D.P.; Duirk, S.E.; Tarr, J.C.; Collette, T.W. Monitoring the speciation of aqueous free chlorine from pH 1 to 12 with Raman spectroscopy to determine the identity of the potent low-pH oxidant. *Appl. Spectrosc.* **2006**, *60*, 764–772. [CrossRef]

78. Atkins, P.W.; De Paula, J. *Atkins' Physical Chemistry*; Oxford University Press: Oxford, UK, 2010; ISBN 978-0-19-954337-3.